

MRI-INDUCED SAR ON PACEMAKER LEADS

Numerical Simulations on Three Human Phantoms

Eugenio Mattei, Giovanni Calcagnini, Michele Triventi, Federica Censi and Pietro Bartolini
Italian National Institute of Health, Department of Technology and Health, Rome, Italy

Keywords: Magnetic Resonance Imaging, Pacemaker, Specific Absorption Rate, Human Visible Dataset.

Abstract: Numerical simulations were performed to evaluate the Specific Absorption Rate (SAR) induced at the tip of a pacemaker (PM) implant by the 64 MHz radiofrequency (RF) field used in 1.5T Magnetic Resonance Imaging (MRI) procedures. The analysis was performed by using a commercial FDTD software (SEMCAD X, SPEAG, Switzerland) and aimed at the evaluation of the impact that the patient's morphology has on the induced local SAR at the implant tip. In particular three human phantoms were studied: a 34-year old man model, a 26-year old woman, and a 6-year old boy. The three phantoms reproduce more than 70 tissues of the human body with a resolution of 1 mm. Inside each phantoms, realistic implant configurations were modelled, considering both left and right pectoral implants, and atrial and ventricular stimulations. The local SAR values at the lead tip was compared for the three phantoms and sensible differences were observed: with a RF excitation set to produce an whole-body average SAR of 2 W/kg without any implants, local SAR values ranged from 641W/kg (woman model – right ventricular implant) to 3 W/kg (boy model – left atrium implant). We also observed that, in general, ventricular implants showed a higher SAR compared to atrial ones, as well as right pectoral implants compared to left ones. However, not always a higher implant area or a longer lead path implied higher SAR at the tip, indicating the coupling mechanisms between the implant and the RF field are likely to be more complex than the only area-dependent induction law.

1 INTRODUCTION

The number of Magnetic Resonance Imaging (MRI) scans performed annually has increased dramatically over the past few years. Parallel to the growth and evolution of the MRI field, is the burgeoning number of patients benefiting from implantable cardiac systems including pacemaker (PM) and implantable cardioverter/defibrillators (ICDs). The combination of these two growing phenomena results in an estimated 50-75% probability of a patient being indicated for an MRI study over the lifetime of their device; it has created an estimated 200,000 implanted patients who were denied the MRI scan, and this numbers are likely to increase in the future (Rougin et al, 2004). Given the rapid expansion of technology in the fields of both MRI and device arrhythmia management, there is increasing interest in the issue of implantable device safety in the MRI environment. For the purpose of MRI, non-ferromagnetic material is available for manufacturing of implantable devices. Considering the impressive progress in the use of diamagnetic

material, the most important safety problem associated with MRI and medical implantable devices is the potential tissue heating induced by the radiofrequency (RF) fields. In this field, numerical studies are crucial to extend the range of experimental measurements and to correlate heating results to those expected in humans. Simulations can be used to model realistic patient geometries, to deliver more information (e.g., 3D fields instead of single measurement points) and to study individually the impact of parameters such as tissue properties, boundary conditions, etc. As the finite difference time domain (FDTD) method has been a widely used technique for characterization of RF heating, it is an excellent candidate to render an accurate estimate of the specific absorption rate (SAR), and therefore heating, due to implantable devices during MRI experiments.

The anatomical structure of the human body as sets of minute elements (voxels) suitable to be imported inside the FDTD environment have been obtained from MRI scans, X-ray computed tomography, or anatomical coloured images of the

Visible Human Project (VHP). These data are today largely available at a high resolution, so that almost all the various human tissues can be taken into account (Visible Human Dataset – VHD).

The purpose of this study is to numerically compute the local SAR induced by a 64 MHz RF coil used in MRI procedures at the lead tip of a PM implant. Local SAR values were compared for three human phantoms: a 34-year-old man model, a 26-year-old woman, and a 6-year-old boy. Inside each phantom, realistic implant configurations were modelled; left and right pectoral implants, as well as atrial and ventricular stimulations were taken into account.

2 METHODS AND MATERIALS

The MRI RF coil model was developed using a commercial FDTD (Finite Difference Time Domain) solver (SEMCAD X, SPEAG, Zurich, Switzerland). It represents a 16-rung low-pass birdcage coil (60 cm high, with an inner radius of 30 cm) which reproduces the RF field generated during MRI procedures (Figure 1).

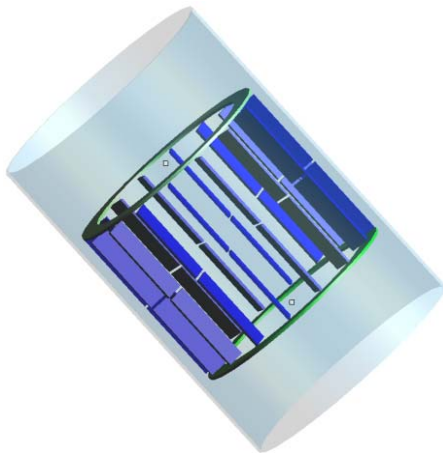


Figure 1: FDTD model of the RF birdcage coil.

Two voltage sources were applied at one of the two external rings of the coil, with a 90° shift both in space and in time. Inside the coil, a uniform and circularly polarized magnetic field was thus generated. An external metal shield was used to limit the RF field inside the birdcage coil.

The human phantoms were imported from “The Virtual Family” package developed by the Foundation for Research on Information Technology in Society (IT²IS Foundation - Zurich, Switzerland). In particular we used:

- The 34-year-old man model;
- The 26-year-old woman;
- The 6-year-old boy model.

Each phantom distinguishes more than 70 tissues with a spatial resolution of 1 mm. The phantoms were placed inside the RF coil and their position was adjusted to have the coil isocenter at the lowest part of the sternum (xiphoid process – Figure 2).

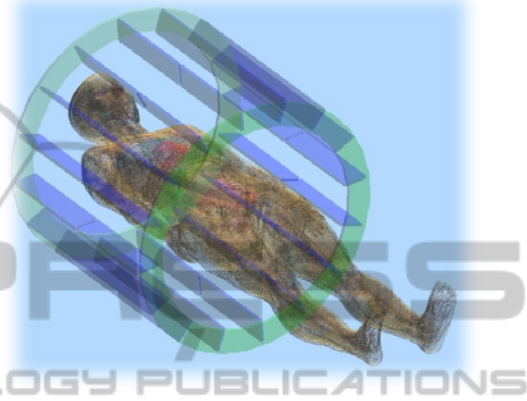


Figure 2: Human phantom (female) inside the birdcage coil.

As PM implant, a bicameral stimulator was modelled in the right and left pectoral regions. The lead path was derived from RX images of patients with a PM implant (Figure 3). Both for atrial and ventricular stimulation, a unipolar lead was modelled as a perfect electric conductor (PEC) thin wire (radius = 0.5 mm) with a silicon insulation of 1.5 mm radius. At the end of the lead, a 1 mm bear PEC tip was put in contact with the heart wall.

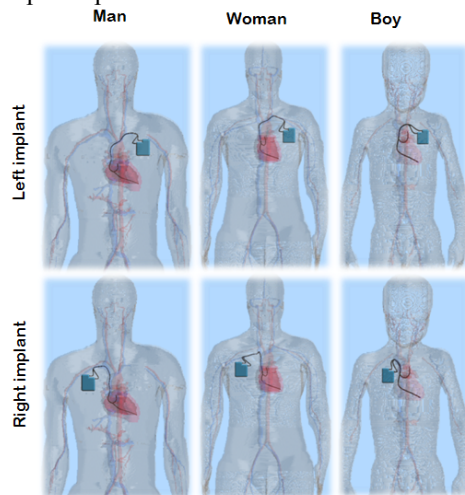


Figure 3: Human phantoms and PM implants.

To obtain the required resolution at the implant, a two-step approach has been employed: a first simulation of the birdcage without the wire is performed using a relatively coarse grid (≈ 15 million cells, graded mesh). The fields are recorded on the surface of a rectangular box around the implant, and are used to excite a second simulation restricted to the area where the PM and its lead are implanted (≈ 20 -30 million cells, graded mesh).

This two-step approach, which is based on Huygens' principle, allows to obtain a high resolution around the implant and to properly model the lead. To ensure the continuity of the inner conductor of the lead and of its insulation a maximal refinement at the lead (0.2-0.6 mm) was needed. The same mesh parameters were used for the three phantoms. In Figure 4 the graded mesh adopted in the area of the implant and the resulting voxel are overlaid to the heart and vessel of the VHD.

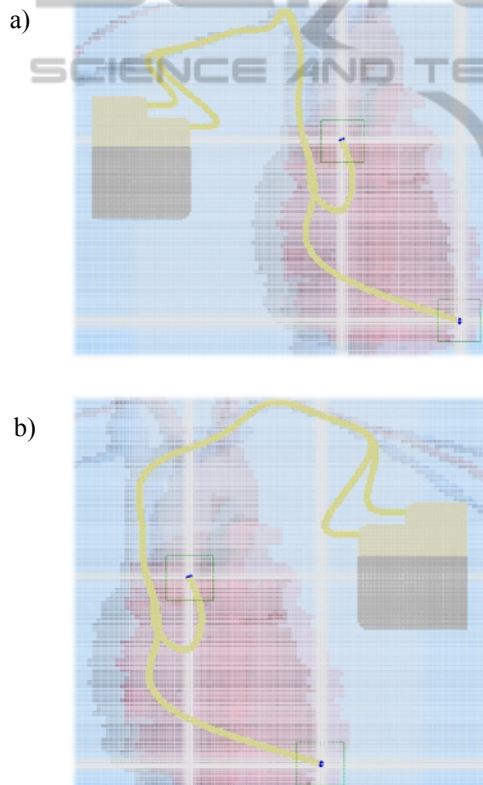


Figure 4: FDTD graded mesh in the area of the PM implant: right pectoral implant (a) and left pectoral implant (b).

Local SAR deposition was calculated from the E-field estimated by the model. SAR was calculated as described in the IEEE1528 standard (IEEE1528, 2006), over a 1mg mass.

A 1 mg mass was chosen as a trade-off between a volume small enough to significantly account for local SAR value, but big enough to prevent misleading results due to computational errors.

3 RESULTS

Figure 5 shows the SAR distribution for the female phantom with the PM in the right pectoral region, exposed to the RF field of the birdcage coil.

Local hot-spots can be observed at the contact points between the two lead tips and the heart wall, in the atrium and in the ventricle. A similar distribution was obtained also for the man and the boy phantoms.

The local SAR values computed for the man, the woman and the boy phantom are reported in Figure 6. The highest SAR was observed at the tip of the right ventricular implant in the woman model (641 W/kg); on the other hand, the boy phantom is the one associated to the lowest SAR values, for all the implant configurations tested.

In general, the right pectoral positioning implies higher SAR compared to left pectoral implants, as well as ventricular stimulation compare to atrial one.

The only exception is represented by the left atrial implant in the woman phantom, which showed higher SAR values than the right atrial one.

In these simulations, the excitation signal applied to the RF coil was not the same for the man, the woman and the boy model, but was adjusted to obtain an average whole-body SAR of 2 W/kg (maximum value allowed during standard MRI procedures) inside all the phantoms.

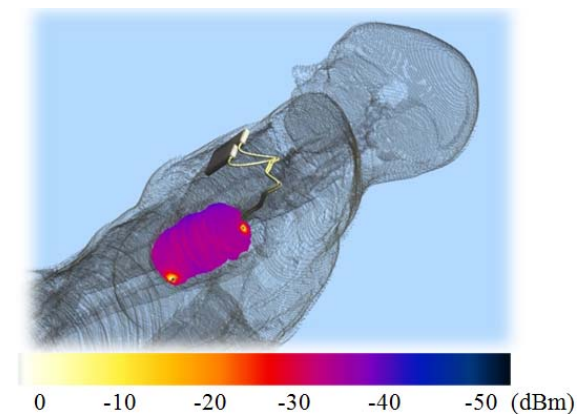


Figure 5: Example of the SAR distribution over the heart surface resulting from the exposure of the implanted phantom to the RF field generated by the birdcage coil. The two hot spots represent the contact points between the lead tips and the heart wall.

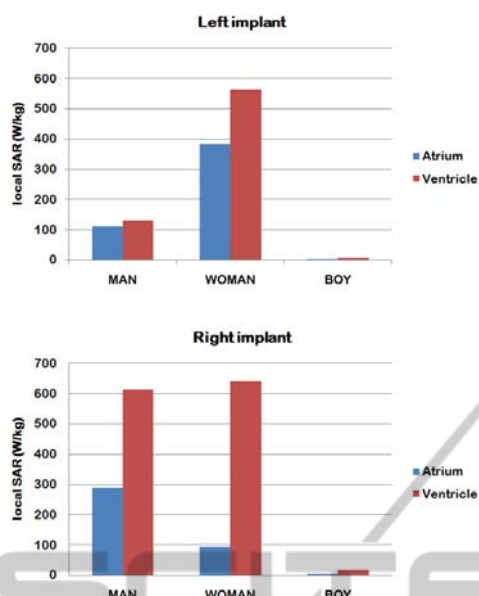


Figure 6: Local SAR values at the PM lead tip for the man, woman and boy phantoms. SAR calculation was averaged over 1 mg mass. The whole body SAR without the implant was 2 W/kg in all the phantoms.

If the amplitude of the signal is not changed, the average SAR significantly differs in the three models: an excitation that produces an average whole body SAR of 2 W/kg in the boy model, for example, leads to an average SAR of 38.5 W/kg in the man phantom, and of 25.9 in the woman phantom.

In order to characterize the lead paths that a realistic PM implant implies in different anatomical structures and in different locations, we calculated the lead length from the connection with the PM chassis to the tip. The data reported in table 1 show how a longer lead does not always imply a higher SAR at the tip.

Table 1: Lead length for the configuration tested inside the man, the woman and the boy phantoms.

Phantom type		Lead length (mm)	
		Atrium	Ventricle
MAN	Left imp.	280	365
	Right imp.	302	381
WOMAN	Left imp.	283	345
	Right imp.	308	369
BOY	Left imp.	148	205
	Right imp.	161	207

4 DISCUSSION

RF induced heating of biological tissue has long been a concern for patients undergoing magnetic resonance imaging (MRI). With regards to the MRI induced heating on PM and ICD leads, a wide database of experimental measurements is now available in literature (Mattei et al, 2008; Nordbeck et al, 2009). However, these studies use simplified model of the human body, typically a rectangular box phantom filled with an homogeneous gel, whose physical properties are defined to closely match those of biological tissues (ASTM F2182-02a). Even when phantoms of more complex shapes are used, they always assume a uniform behaviour of human tissues and do not take into account the realistic anatomical structure of the human body. In addition, the large number of variables that take part in the process may often result in a loss a general validity, requiring additional efforts to perform extensive and exhaustive measurements. Thus, modellistic approaches based on numerical tools might represent a useful mean, able to overcome such limitations.

In this study we compared the RF-induced SAR during MRI scans at the lead tip of a PM implanted in human models that thoroughly reproduce the anatomical structures of an adult male, an adult woman and a boy. Realistic implant configurations markedly differ for the three phantoms, in terms of lead length, path, and area covered by the implant. Thus, it is not surprising that also the local SAR induced at the lead tip sensibly varies in the simulations we performed. However, there are several aspects that suggests how the coupling mechanisms between the RF field and the PM implant is much more complex than it may appear.

Several papers in the literature (Sommer et al, 2000, Rezai et al, 2005) chose a configuration of the pacemaker lead in the coronal plane to achieve a maximal magnetic induction area in order to maximize the heating at the lead tip. We found that the induced SAR is not always proportional to this area. In particular, in the comparison between left and right implant configurations, right implants covered an area significantly smaller than the left counterparts and the SAR is generally higher for the former than the latter ones.

The lead length seems to be a parameter that better correlates with the induced SAR (right implant implies longer leads than left ones), but also in this case, simulated data highlight some exceptions: in particular, the highest SAR was observed at the tip of the right ventricular implant in

the woman model, which has a shorter lead length than the counterpart in the man model. Thus, there should be other aspects related to the morphology of the human phantom that can affect the amount of the deposited power and consequently the tissue heating at the lead tip; such aspects may involve the particular path the lead follows inside the human tissues and the electromagnetic field distribution induced during MRI scans in the same regions.

5 CONCLUSIONS

The present numerical study shows how the differences in terms of patient's anatomy (different gender and age) have an impact on the MRI induced SAR, and consequently tissue heating, at the tip of an implanted PM lead. It is justified by the changing in lead path and electromagnetic field distribution that different anatomical models imply. Our data show also that the implant area or lead length are not the only parameters that can affect the amount of induced heating the implant tip, but more complex coupling phenomena must be taken into account.

Roguin A, Zviman MM, Meininger GR, Rodrigues ER, Dickfeld TM, Bluemke DA, Lardo A, Berger RD, Calkins H, Halperin HR. Modern pacemaker and implantable cardioverter/defibrillator systems can be magnetic resonance imaging safe: in vitro and in vivo assessment of safety and function at 1.5 T. *Circulation*. 2004 Aug 3;110(5):475-82.

Sommer T, Vahlhaus C, Lauck G, von Smekal A, Reinke M, Hofer U, Block W, Traber F, Schneider C, Gieseke J, Jung W, Schild H. MR imaging and cardiac pacemakers: in-vitro evaluation and in-vivo studies in 51 patients at 0.5 T. *Radiology* 2000 Jun;215(3):869-79

REFERENCES

- ASTM F2182-02a – “Standard Test Method for Measurement of Radio Frequency Induced Heating Near Passive Implants During Magnetic Resonance Imaging”, *ASTM International*, 100 Barr Harbor Drive, PO Box C700, West Conshohocken, PA, 19428-2959 USA
- IEEE, IEEE1528, recommended practice for determining the spatial-peak specific absorption rate (SAR) in the human body due to wireless communications devices: Measurement techniques, *IEEE Standards Department* 52(5), 1 2006
- Mattei E, Triventi M, Calcagnini G, Censi F, Kainz W, Mendoza G, Bassen HI, Bartolini P. Complexity of MRI induced heating on metallic leads: experimental measurements of 374 configurations *Biomed Eng Online*. 2008 Mar 3;7:11
- Nordbeck P, Weiss I, Ehses P, Ritter O, Warmuth M, Fidler F, Herold V, Jakob PM, Ladd ME, Quick HH, Bauer WR. Measuring RF-induced currents inside implants: Impact of device configuration on MRI safety of cardiac pacemaker leads. *Magn Reson Med*. 2009 Mar;61(3):570-8.
- Rezai AR, Baker KB, Tkach JA, Phillips M, Hrdlicka G, Sharan AD, Nyenhuis J, Ruggieri P, Shellock FG, Henderson J. Is magnetic resonance imaging safe for patients with neurostimulation systems used for deep brain stimulation? *Neurosurgery* 2005 Nov;57(5):1056-62